

Photometric Calibrations of Gemini Images of NGC 6253

Sean Pearce

A senior thesis submitted to the faculty of
Brigham Young University
in partial fulfillment of the requirements for the degree of
Bachelor of Science

Elizabeth Jeffery, Michael Joner, Advisors

Department of Physics and Astronomy

Brigham Young University

April 2018

Copyright © 2018 Sean Pearce

All Rights Reserved

ABSTRACT

Photometric Calibrations of Gemini Images of NGC 6253

Sean Pearce

Department of Physics and Astronomy, BYU
Bachelor of Science

To better understand the effects of high metallicity on white dwarf cooling processes, especially the white dwarf cooling age, we have analyzed images of the metal-rich open cluster NGC 6253, from the 8 m Gemini-South Observatory. To standardize the Gemini photometry of the cluster, we have also secured imaging data of both the cluster and standard star fields using the 0.6 m SARA Observatory at Cerro Tololo Inter-American Observatory. By comparing the photometric magnitudes and colors of additional stars in standard star fields of both the SARA data and the published Gemini zero-points of the standard star fields, we calibrated the data obtained for the cluster. These calibrations are an important part of the project to obtain a standardized deep color magnitude diagram and white dwarf luminosity function to analyze the cluster. With the standardized color magnitude diagram, we determined the cluster's main sequence turnoff age to be 4.6 ± 0.2 Gyr., much older than the earlier results showing an age ~ 3.6 Gyr. Because the cluster is much older than expected, the white dwarfs have cooled and dimmed beyond our limits of detection. Since we were unable to detect the coolest white dwarfs, we could not make a white dwarf luminosity function with the current data set.

Keywords: techniques: photometric — white dwarfs — open clusters and associations: general

Contents

Table of Contents	iii
List of Figures	iv
1 Introduction	1
1.1 Star Clusters	1
1.2 Stellar Evolution	2
1.3 Hertzsprung-Russell Diagrams and Color Magnitude Diagrams	3
1.4 White Dwarfs and White Dwarf Luminosity Functions	6
1.5 Metallicity	8
1.6 NGC 6791	8
1.7 NGC 6253	10
2 Observations and Calibrations	11
2.1 Gemini Images	11
2.2 Standardization	12
2.2.1 SARA Images	12
2.3 Verification	14
3 Results and Discussion	16
3.1 Standardized Color Magnitude Diagram	16
3.2 Further Study	17
Appendix A Data Reduction in THELI	20
Bibliography	32

List of Figures

1.1	A Hertzsprung-Russel Diagram with many well known stars from the Milky Way	4
1.2	A color magnitude diagram of M15	5
1.3	Luminosity function of galactic disk white dwarfs derived from the Sloan Digital Sky Survey	7
1.4	Data of NGC 6791 compiled by Bedin et al. (2008)	9
2.1	NGC 6253 with the stars used as local standards marked	14
3.1	Standardized color magnitude diagrams of NGC 6253	17
3.2	Standardized color magnitude diagram of NGC 6253, with the isochrone fit overlaid	18
3.3	Full standardized color magnitude diagram, with the isochrone fit overlaid and theoretical locations of white dwarfs	19
A.1	Example directory for use in THELI	20
A.2	Initialise tab within THELI	21
A.3	Preparation tab within THELI	22
A.4	Calibration tab within THELI	23
A.5	Background tab within THELI	24
A.6	Weighting tab within THELI	25
A.7	Astrom / Photom tab within THELI, before running	26

A.8 Parameters used for the Create Source Cat task	27
A.9 Parameters used for the Astro+Photometry task	28
A.10 Astrom / Photom tab within THELI, after running	29
A.11 Coaddition tab within THELI	30
A.12 The coadd_null subdirectory	31

List of Tables

2.1	A summary of observations taken of NGC 6253 on the Gemini-South telescope with the imaging channel of the Gemini MultiObject Spectrograph (GMOS)	11
2.2	A summary of observations taken of NGC 6253 and standard fields (Smith et al. 2007) from the SARA telescope	13
2.3	A summary of observations taken of standard star fields (Smith et al. 2007) from the Gemini archive in the Canadian Astronomy Data Centre	15

Chapter 1

Introduction

Astronomical research is limited in ways that many other sciences are not. We do not have the capability of using a laboratory to create stars or galaxies with our desired conditions. Instead, we must find case studies in the universe. Star clusters give us an excellent analog to laboratories, as the stars within a cluster have the same age, chemical composition, and are the same distance from us.

This chapter describes star clusters and some methods used to analyze them, namely color magnitude diagrams and white dwarf luminosity functions. It then explains some of the research that has been done on the open cluster NGC 6791 and why that cluster has inspired our research of NGC 6253. It also gives background information on that cluster.

1.1 Star Clusters

To better understand why star clusters are so useful, it would be good to understand what a star cluster actually is. A star cluster is a population of stars that formed from the same cloud of gas and dust. There are two main types: globular clusters and open clusters. Globular clusters tend to be very old—often around 12-13 billion years old, usually containing some of the oldest stars in

their host galaxies. They can contain millions of stars, in a roughly spherical distribution. Open clusters, on the other hand, tend to be much younger, only a few billion years old or less, and their stars have a much looser, amorphous distribution. They tend to only contain a few hundred stars.

Because each cluster formed from the same gas and dust cloud, the stars within them have identical compositions¹. Stars within a cluster also have the same age and are the same distance from us; any differences in their ages and distances are insignificant compared to the total age and distance. The stars within the clusters differ only in their masses. Because stars of different masses evolve at different rates, star clusters give us the chance to see how evolution progresses, since there are stars at various stages present, making them very useful tools for studying evolutionary processes.

1.2 Stellar Evolution

Before we discuss the various methods for analyzing star clusters, it will be useful to understand some basics of stellar evolution. Stars form out of clouds of gas and dust in the universe. As these clouds collapse into thousands or even millions of stars, the gravitational potential energy of the molecules within them is converted to heat. If the temperatures and pressures get high enough then these proto-stars can initiate fusion of hydrogen into helium in their cores. Once this begins, stars will rapidly stabilize, with this stage of life called the main sequence. Here they will stay until they have fused all of the hydrogen in their cores. For the most massive stars, this process will take only a few million years; for the least massive possibly a trillion years—the time scales are such that these stars have never been observed beyond the main sequence; the Universe is simply not old enough. The more massive the star, the more rapidly it can fuse its hydrogen; so while the larger stars have much more fuel to burn, they can get through it far faster than the smaller stars.

¹This is true for open clusters (Feng & Krumholz 2014); new research is emerging that this may not always be true for globular clusters (Bekki 2011; Milone et al. 2016).

At this point the processes differ between high-mass stars and low-to-medium-mass stars. The high-mass stars will eventually become neutron stars or black holes, which are outside the scope of this project, so we will focus on the evolution of the small and medium stars. Once the stars have finished fusing the hydrogen in their cores, they cease to have the stability of the main sequence. Stars will begin to fuse hydrogen outside the core, and slowly expand and cool, becoming Red Giants. As more and more hydrogen from above the core burns to helium and settles in the core, the core temperatures and pressures will increase until eventually they become hot enough to begin fusing helium into carbon and oxygen.

Once this occurs, the outer layers of the star will contract and heat up, moving the star into what is called the Horizontal Branch stage of evolution (the name will make more sense after we discuss Hertzprung-Russell Diagrams in the next section). Here the star will remain until the helium in its core is expended, leaving a core of carbon and oxygen. At this point the star goes into what is called the Asymptotic Giant Branch, which is similar to the Red Giant Branch except that instead of a helium core with a hydrogen burning shell around it, it now has a carbon-oxygen core, with a helium burning shell around it, and a hydrogen burning shell around that.

The stars in the Asymptotic Giant Branch are unstable and will eventually run out of fuel to burn, as they are not massive enough for carbon fusion to begin in their cores. Once the fuel has run out, these stars will shed their outer layers—which are now called planetary nebulae—and leave behind only their naked cores, called white dwarfs, which will be discussed later in this chapter.

1.3 Hertzprung-Russell Diagrams and Color Magnitude Diagrams

Hertzprung-Russell (H-R) Diagrams are scatter plots of stellar surface temperatures against their luminosities (the amount of light they give off). These diagrams can be very useful, partic-

ularly for describing stellar evolution. Figure 1.1 shows various well known stars from the Milky Way plotted on an H-R diagram. The main sequence stars lie along the diagonal in the middle, the red giant branch then moves off to the right, and the white dwarfs sit low and to the left.

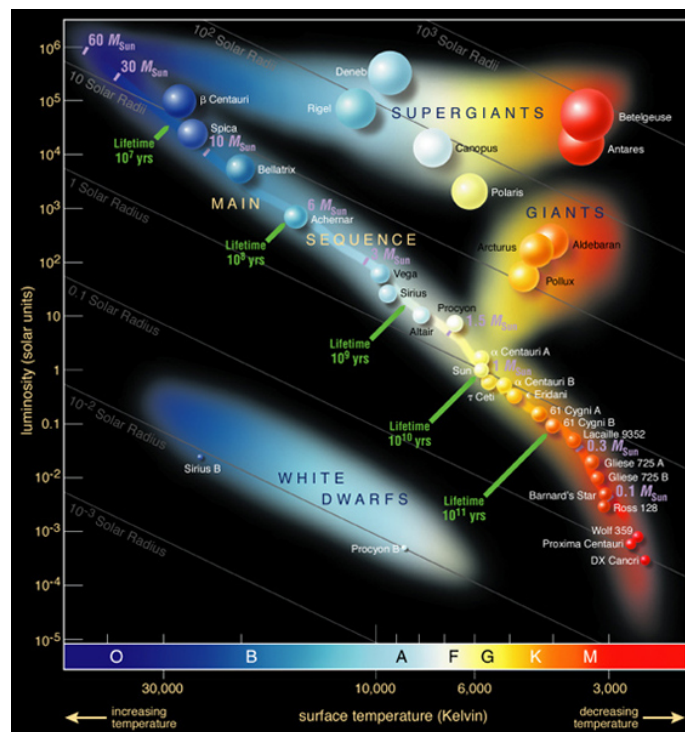


Figure 1.1 A Hertzsprung-Russell Diagram with many well known stars from the Milky Way (ESO Accessed 26 August 2017).

H-R diagrams, while very useful, can be difficult to create. A star's temperature and luminosity cannot be observed directly, only calculated using other properties that can be observed directly. Two of these observable properties are color (which can be used in place of temperature) and apparent magnitude (the brightness of the star as seen from Earth, which, when combined with distance, is related to luminosity). Because these values are easier to obtain, special H-R Diagrams with these analogs are used, called color magnitude diagrams. As can be seen in Figure 1.2, a color magnitude diagram shows the same features as H-R diagrams, with the smaller stars in the bottom half still along the main sequence, and the larger stars near the middle turning off into the

red giant branch. The horizontal branch moves back to the left of the red giants, along a horizontal line (which is what gives them their name), and the asymptotic giant branch runs parallel to the giants, only slightly higher.

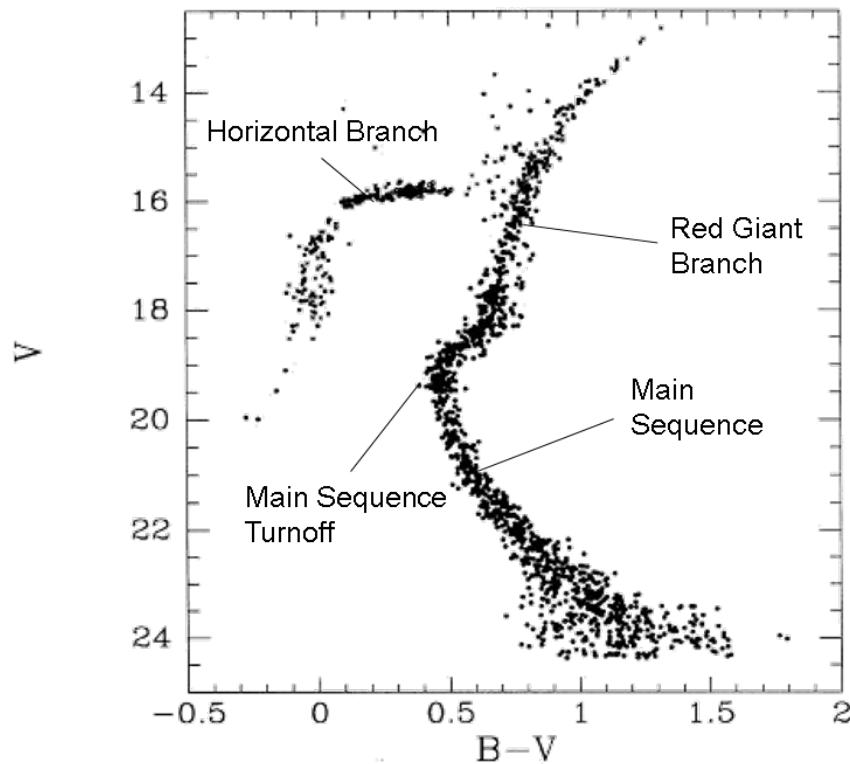


Figure 1.2 A color magnitude diagram of M15 (Durrell & Harris 1993). Annotations have been added to show the various stages of evolution.

Because the lifetime of main sequence stars is determined by nuclear reaction rates, which are well understood, the main sequence lifetime of stars of a given mass can be calculated. Knowing this, we can determine the age of stars in a cluster based on where the turnoff to the red giant branch appears on the color magnitude diagram. This is referred to as a main sequence turnoff age. The primary method for calculating this age is through the use of computer models called isochrones. These models allow for the user to input various parameters (such as distance and composition) into a simulated star cluster with stars of a wide variety of masses. The model then simulates the

evolution of that cluster through time, with the stars all aging together, and determines the color and apparent magnitude of the stars in the cluster. By comparing the predicted distribution of the stars from the isochrone on the color magnitude diagram with the observed data, and finding the simulated age that gives the best fit, we can accurately find the age of the cluster.

1.4 White Dwarfs and White Dwarf Luminosity Functions

As was previously stated, white dwarfs are the remnants of small and medium stars—though none of the small stars have yet aged beyond the main sequence, so all of the white dwarfs we find in the universe are remnants of medium stars. When these stars finish their evolution, they shed their outer layers and leave behind their bare cores. These remnants are extremely dense—with their masses being on the same order as the Sun, but their volumes much closer to that of the Earth—being supported by electron degeneracy pressure. Because there is no longer any fusion occurring in these objects, their brightness is entirely from residual heat, and they dim over time as they cool via Newton’s Law of Cooling.

This predictable dimming gives us another method to calculate the age of a cluster. Plotting the number of white dwarfs in a given luminosity interval gives us a white dwarf luminosity function. The exponential decay described by Newton’s Law of Cooling predicts that these objects initially cool very rapidly, then the cooling rate decreases as time goes on. Because of this the stars tend to pile up in the white dwarf luminosity function in the dimmest luminosity interval, causing a peak in the plot before a sharp drop-off, as can be seen in Figure 1.3. Finding the temperature of the white dwarfs at the peak, and knowing the approximate initial temperature, we can calculate the time that has passed since the star became a white dwarf, and, therefore, the age of the cluster. In populations old enough to form a significant number of white dwarfs, the cooling age of the coolest white dwarf is much greater than the pre-white dwarf stages of the star.

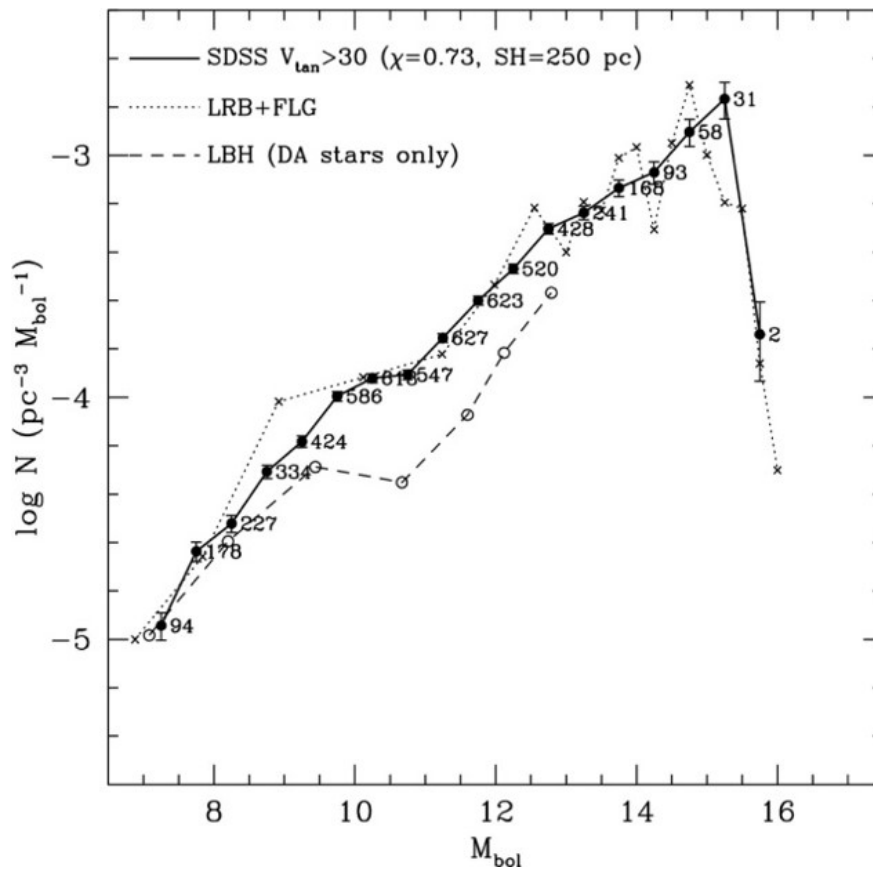


Figure 1.3 Luminosity function of galactic disk white dwarfs derived from the Sloan Digital Sky Survey (SDSS), from Harris et al. (2006), compared to the luminosity functions of Leggett et al. (1998) and Liebert et al. (2005). Compiled by Garcia-Berro and Oswald (2016).

1.5 Metallicity

One last concept that will be helpful to understand before describing the clusters in this study is metallicity. Metallicity describes a star's or stellar population's chemical composition. In astronomy, we define a metal to be all elements heavier than helium on the periodic table. The most commonly used notation for metallicity is $[\text{Fe}/\text{H}]$, which compares the abundance of iron to hydrogen and is defined as

$$[\text{Fe}/\text{H}] = \log_{10} \left(\frac{N_{\text{Fe}}}{N_{\text{H}}} \right)_{\text{star}} - \log_{10} \left(\frac{N_{\text{Fe}}}{N_{\text{H}}} \right)_{\text{Sun}} \quad (1.1)$$

where N is the abundance of the element. By definition, the Sun has an $[\text{Fe}/\text{H}]$ value of zero; a positive value indicates a higher metallicity than the Sun (i.e. a higher abundance of heavy elements), and a negative value indicates a lower metallicity.

1.6 NGC 6791

NGC 6791 is an old, metal-rich open cluster. Its main sequence turnoff age is approximately 8 Gigayears (Gyr) and its metallicity is approximately $[\text{Fe}/\text{H}] \sim +0.40$ (Carraro et al. 2006; Gratton et al. 2006; Origlia et al. 2006), or about two and a half times the metallicity of the Sun. When Bedin et. al. (2008) obtained images deep enough to see the full white dwarf sequence and make a white dwarf luminosity function, they found strange anomalies. Instead of a single peak, they found two, as seen in the far right panel of Figure 1.4. Furthermore, the first peak would indicate that the cluster is only 4 Gyr, and the second, 6 Gyr; neither agreeing with the main sequence turnoff age.

García-Berro et al. (2010) and Althaus et al. (2010) have explained the double peak as simply being a result of unresolved binaries (two white dwarfs orbiting close enough to each other that the telescope could not separate them). However, they have hypothesized that the slowed cooling

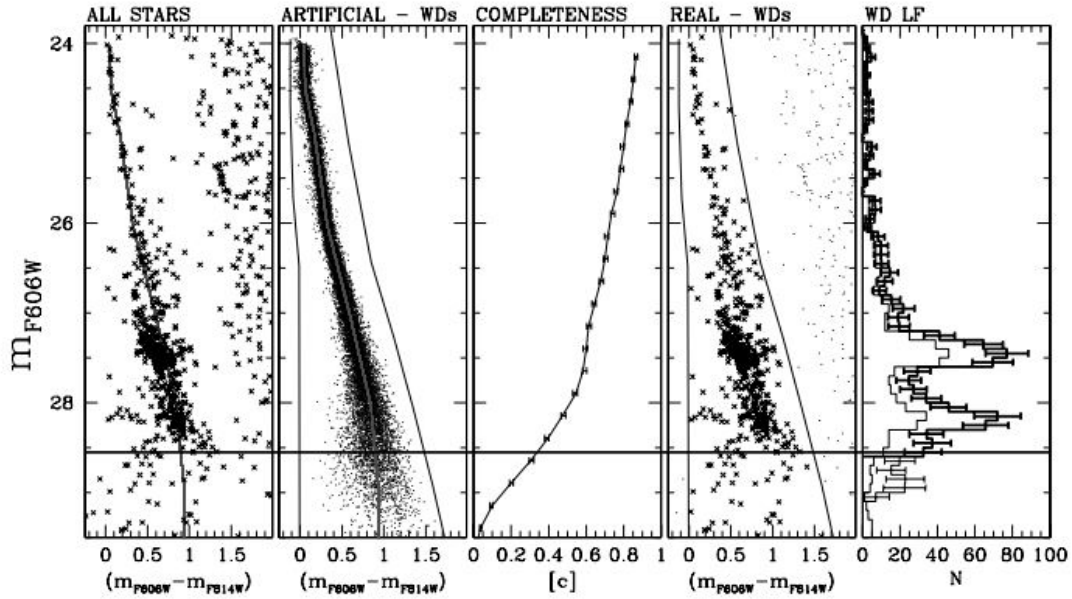


Figure 1.4 Data of NGC 6791 compiled by Bedin et al. (2008), with the white dwarf luminosity function in the far right panel. The first and fourth panels show the color magnitude diagram of the cluster, focused on the white dwarfs. An increased density of stars in these two panels can be seen at magnitudes lining up with the peaks in the white dwarf luminosity function. The second and third panels are unimportant for this project.

may be due to the high metallicity of the cluster. ^{22}Ne , a byproduct of helium fusion, is present in high enough quantities in metal-rich stars that its settling into the center of the white dwarf releases gravitational potential energy as heat, slowing cooling at moderate luminosities. Then, at lower luminosities, carbon-oxygen phase separation can cause a similar effect. If this is the case, it could have important implications on how we understand stellar evolution, particularly mass loss and white dwarf cooling, as well as impacting age calculations using white dwarf luminosity functions. This question is the primary motivation for our study of NGC 6253, a similarly metal-rich open cluster, described in the next section.

1.7 NGC 6253

NGC 6253 is another relatively old, metal-rich open cluster. Its metallicity has been measured at $[\text{Fe}/\text{H}] \sim +0.43$ (Anthony-Twarog et al. 2010) and its age has most recently been measured to be 3.5 Gyr (Montalto et al. 2009) or 3.8-4.6 Gyr (Rozycka et al. 2014). This makes the cluster very similar to NGC 6791 in metallicity, and old enough to have a significant number of white dwarfs, and a great candidate for testing hypotheses about the white dwarf luminosity function anomaly. Because this cluster sits only 6.251 degrees below the galactic plane, there is a high contamination of foreground and background stars, making it difficult to study. As such, no data have been taken deep enough to see the full white dwarf sequence.

Our aim is to obtain and standardize images of this cluster deep enough to create a white dwarf luminosity function and see if it shows a similar delayed cooling. The results of this study could provide important validation or refutation to the hypothesis that high metallicity causes slowed cooling in white dwarfs. Chapter 2 describes our process of obtaining and calibrating images of this cluster, and our process of verifying our calibration methods. Chapter 3 presents our standardized color magnitude diagram, what we learn from it, and the next steps in our research.

Chapter 2

Observations and Calibrations

To create a standardized color magnitude diagram and white dwarf luminosity function for NGC 6253, we needed to obtain high resolution, calibrated cluster images. This chapter explains how we obtained those images and the processes we used to calibrate them.

2.1 Gemini Images

No observations of NGC 6253 have gone deep enough to see the white dwarfs, so our first step was to obtain these images. We did this via queue observing from the 8 m Gemini-South telescope with the imaging channel of the Gemini MultiObject Spectrograph (GMOS). The data taken are summarized in Table 2.1.

Table 2.1 A summary of observations taken of NGC 6253 on the 8m Gemini-South telescope with the imaging channel of GMOS.

Field	Filters	Exp Time (sec.)	Date
NGC 6253	i	3x5	3 June 2013
NGC 6253	i	3x30	3 June 2013
NGC 6253	g	5x5	15 June 2013
NGC 6253	g	3x60	15 June 2013

We reduced these images with bias subtraction and flat fielding using a software package called THELI (Schirmer 2013), as described in Appendix A.

2.2 Standardization

Since there are no standard stars in the images of NGC 6253, we had no way to directly calibrate the images; and without calibrated data, we could not create a standardized color magnitude diagram and white dwarf luminosity function.

2.2.1 SARA Images

To work around this problem, we obtained images from the 0.6 m Southeastern Association for Research in Astronomy (SARA) telescope at the Cerro Tololo Inter-American Observatory (CTIO) to calibrate the Gemini cluster images. We obtained observations, via remote observation, of both NGC 6253 and standard star fields identified by Smith et al. (2007). The observations taken are summarized in Table 2.2.

We reduced the data in IRAF using bias and dark subtraction and flat fielding with IRAF's ZEROCOMBINE, DARKCOMBINE, FLATCOMBINE, and CCDPROC tasks within the noao/imred/ccdred packages. After reducing the images, we found the instrumental magnitudes—the uncalibrated brightnesses—of the standard stars using IRAF's PHOT task in the noao/digiphot/apphot package. We then ran these instrumental magnitudes through the MKIMSET and MKNOBSFILE tasks in the noao/digiphot/photcal package. Then, using the transformation equations from Smith et al. (2007)—which compare the instrumental magnitudes of stars in a field to their standardized magnitudes in the catalogue—and the MKCONFIG task in noao/digiphot/photcal, we created configuration files which were then used in the task FITPARAMS in the same package to solve the transformation equations. With the transformation equations solved, we applied the solution

Table 2.2 A summary of observations taken of NGC 6253 and of standard fields (Smith et al. 2007) from the SARA telescope.

Field	Filters	Exp Time (sec.)	Date
NGC 6253	<i>g/r/i</i>	5x (60/30/30)	22 August 2016
NGC 6253	<i>g/r/i</i>	5x (300/300/300)	22 August 2016
220000-595900-F1	<i>g/r/i</i>	90/60/60	22 August 2016
220000-595900-F1	<i>g/r/i</i>	180/120/120	22 August 2016
220000-595900-F1	<i>g/r/i</i>	180/150/150	22 August 2016
220000-595900-F2	<i>g/r/i</i>	150/100/100	22 August 2016
220000-595900-F2	<i>g/r/i</i>	150/120/120	22 August 2016
PG1633+099-F1	<i>g/r/i</i>	210/180/180	22 August 2016
LSE_259-F1	<i>g/r/i</i>	180/150/150	22 August 2016
180000-600000-F1	<i>g/r/i</i>	2x (150/120/120)	22 August 2016
180000-600000-F2	<i>g/r/i</i>	2x (180/150/150)	22 August 2016
180000-600000-F5	<i>g/r/i</i>	2x (210/180/180)	22 August 2016
E8a-F1	<i>g/r/i</i>	210/180/180	22 August 2016
E8a-F2	<i>g/r/i</i>	210/180/180	22 August 2016
NGC 6253	<i>g/r/i</i>	3x (60/30/30)	21 May 2017
NGC 6253	<i>g/r/i</i>	3x (300/300/300)	21 May 2017
PG1633+099-F1	<i>g/r/i</i>	4x (210/180/180)	21 May 2017
LSE_259-F1	<i>g/r/i</i>	210/150/150	21 May 2017
E8a-F1	<i>g/r/i</i>	210/180/180	21 May 2017

to both the standard field and cluster images using the tasks MKOBSFILE and INVERTFIT in the noao/digiphot/photcal package to find the standard magnitudes for the stars in the cluster images. Then, with the standardized SARA images of NGC 6253, we identified a subset of stars, shown in Figure 2.1, which we cross checked against known variable stars in the field (de Marchi et al. 2010; Kaluzny et al. 2014) to ensure we were selecting stars with non-varying magnitudes to serve as local standards to directly calibrate the Gemini cluster images.

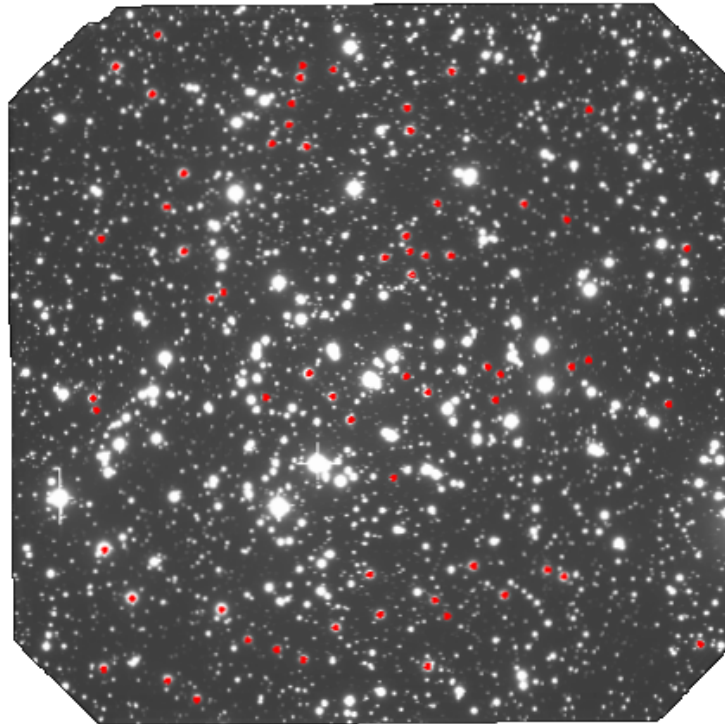


Figure 2.1 Field of NGC 6253 taken with GMOS. The stars used as local standards marked in red.

2.3 Verification

To verify this method, we searched the Gemini archives in the Canadian Astronomy Data Centre¹ to find images of the same standard star fields identified by Smith et al. (2007) from GMOS. The data used are summarized in Table 2.3.

After downloading these images and reducing them in THELI, we found the instrumental magnitudes and standard magnitudes in IRAF using the same process as for the SARA images, described above. We then identified a subset of stars in each of these standard fields to compare with the magnitudes of the same stars in the SARA standard field images. Comparing the magnitudes of these stars, we found a systematic offset of ~ 0.03 magnitude, which we are investigating further. However, this offset is well within our error limit and so does not appreciably affect our data.

¹<http://www.cadc-ccda.hia-ihp.nrc-cnrc.gc.ca/en/search/?collection=GEMINI&noexec=true>

Table 2.3 A summary of observations taken of standard star fields (Smith et al. 2007) from the Gemini archive in the Canadian Astronomy Data Centre.

Field	Filters	Exp Time (sec.)	Date
180000-600000_F1	g/r/i	5.5/4.5/5.5	10 June 2011
180000-600000_F1	g/r/i	5.5/4.5/5.5	06 May 2012
180000-600000_F2	g/r/i	5.5/4.5/5.5	04 July 2011
180000-600000_F2	g/r/i	5.5/4.5/5.5	10 June 2011
180000-600000_F5	g/r/i	5.5/4.5/5.5	13 August 2010
180000-600000_F5	g/r/i	5.5/4.5/5.5	02 November 2010
180000-600000_F5	g/r/i	5.5/4.5/5.5	07 October 2011
220000-595900_F1	g/r/i	5.5/4.5/5.5	02 November 2010
220000-595900_F1	g/r/i	5.5/4.5/5.5	22 November 2012
220000-595900_F2	g/r/i	5.5/4.5/5.5	08 May 2010
E8aF1	g/r/i	5.5/4.5/5.5	06 August 2010
E8aF1	g/r/i	5.5/4.5/5.5	13 August 2010
E8aF1	g/r/i	5.5/4.5/5.5	10 June 2011
E8aF2	g/r/i	5.5/4.5/5.5	09 July 2010
E8aF2	g/r/i	2x (5.5/4.5/5.5)	05 March 2011
E8aF2	g/r/i	5.5/4.5/5.5	04 May 2011
E8aF2	g/r/i	5.5/4.5/5.5	29 June 2013
LSE_259-F1	g/r/i	5.5/4.5/5.5	16 October 2012
LSE_259-F1	g/r/i	5.5/4.5/5.5	29 June 2013
LSE_259-F1	g/r/i	5.5/4.5/5.5	12 September 2013
PG1633+099	g/r/i	5.5/4.5/5.5	02 June 2012

Chapter 3

Results and Discussion

3.1 Standardized Color Magnitude Diagram

Using the standardized cluster images from the Gemini telescope, we produced a standardized color magnitude diagram. To account for the high contamination of foreground and background stars in the cluster images, we needed to identify which of the stars were actual cluster members before we could do any analysis of the data. To accomplish this, we used the data from Montalto et al. (2009), in which they catalogued the proper motions of the stars in the field to find probable cluster members. Figure 3.1 shows the standardized color magnitude diagram both with and without the probable cluster members marked.

Using only the stars identified as probable cluster members, we fit an isochrone (Dotter et al. 2008) to the data to determine a main sequence turnoff age for the cluster with the software suite Bayesian Analysis of Stellar Evolution in Nine Variables (BASE-9; con Hippel et al. 2006; 2014). The resulting color magnitude diagram with the isochrone fit is shown in Figure 3.2.

With this analysis, we found a main sequence turnoff age of 4.6 ± 0.2 Gyr, which agrees well with the main sequence turnoff age found by Rozyczka et al. (2014). With this age, we would

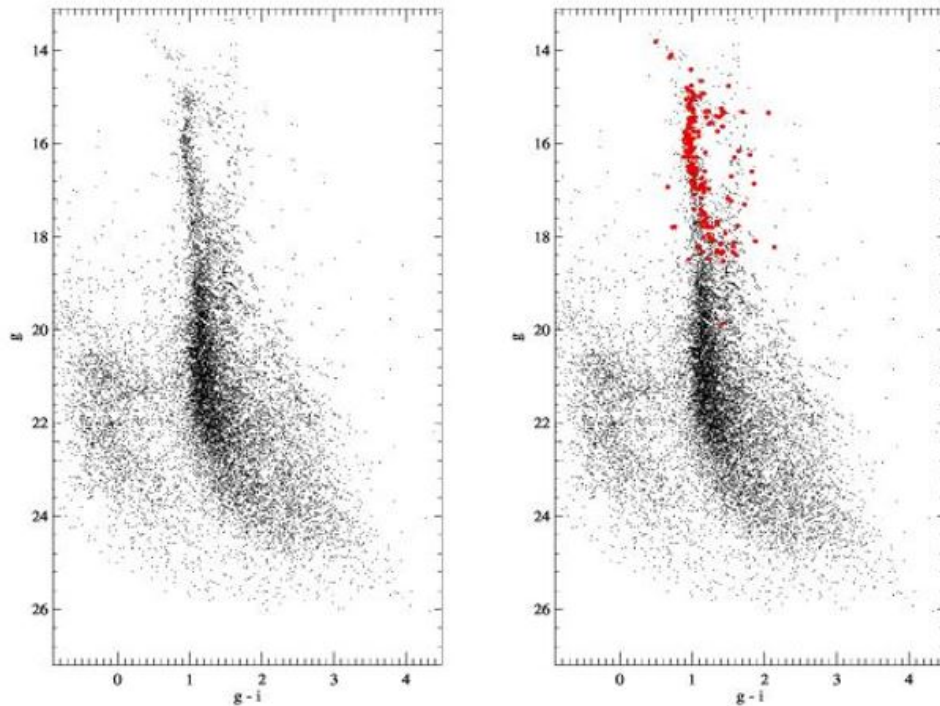


Figure 3.1 Standardized color magnitude diagrams of NGC 6253. The diagram on the right includes the stars identified by Montalto et al. (2009) as probable cluster members in red.

expect the white dwarfs to have dimmed to around magnitude 27, as shown in Figure 3.3. However, our observations were made in 2013, with the age assumed to be that found by Montalto et al. (2009), 3.5 Gyr. As such our observations only went to magnitude 26, where we expected the coolest white dwarfs to be. This means that our observations do not detect the end of the white dwarf sequence, as the coolest white dwarfs have dimmed beyond our limits of observation. We were therefore not able to make a white dwarf luminosity function for the cluster.

3.2 Further Study

As our data did not go deep enough to obtain the full white dwarf sequence, we are currently in the process of applying for new, deeper images of the cluster from the Gemini-South telescope.

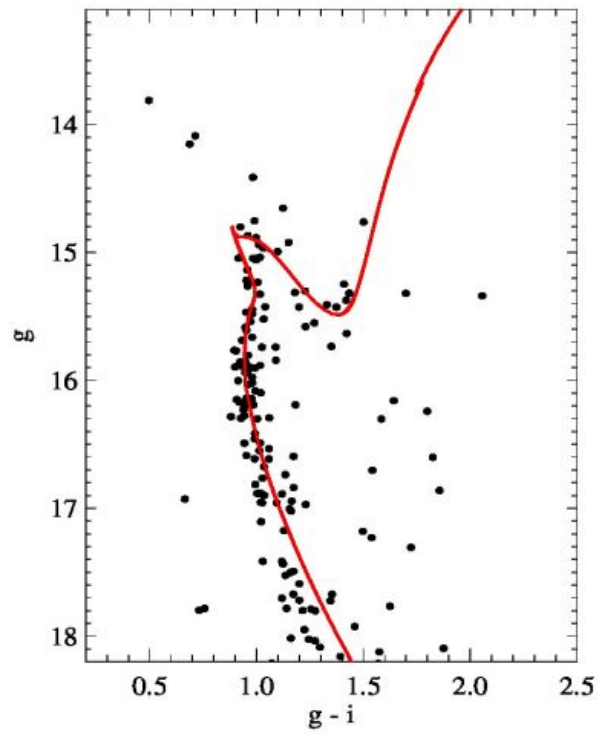


Figure 3.2 Standardized color magnitude diagram of NGC 6253, using only the stars identified by Montalto et al. (2009) as probable cluster members. Overlaid is an isochrone (Dotter et al. 2008) found using the BASE-9 software suite. The isochrone indicates a main sequence turnoff age of 4.6 ± 0.2 Gyr.

With additional data, we should be able to create a white dwarf luminosity function for NGC 6253, which will greatly aid our understanding of stellar evolution in metal-rich stars. As we wait for our proposal to go through, we continue to standardize more SARA images, increasing the reliability of our calibrations. With more data in our calibrations, the systematic offset discussed in Section 2.2 should be reduced or even eliminated.

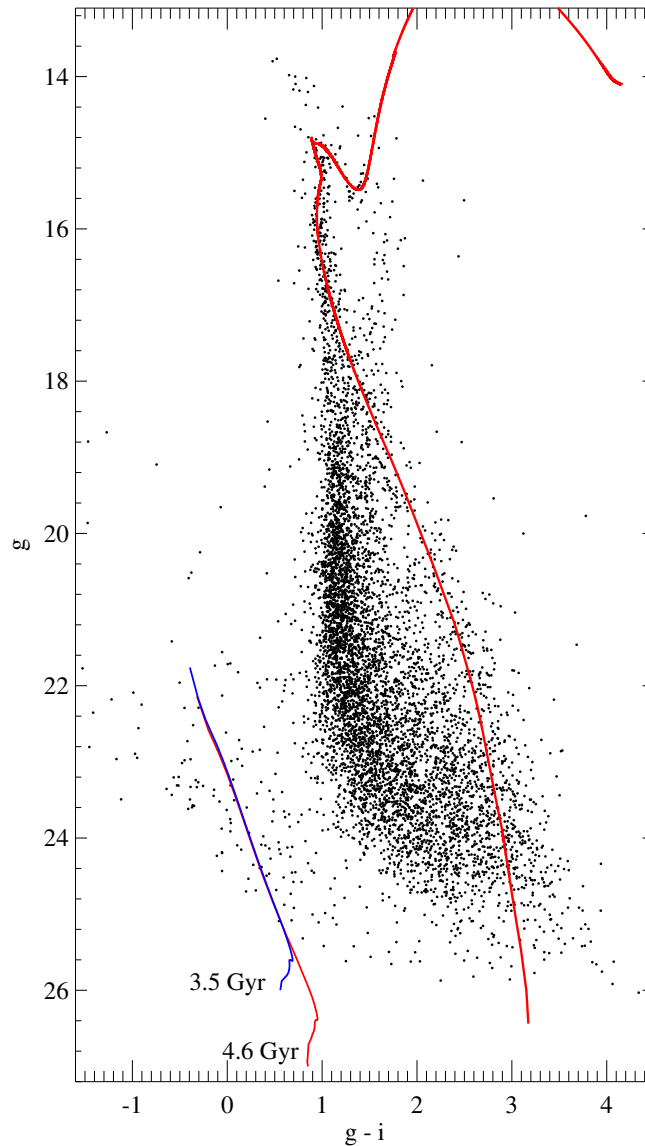


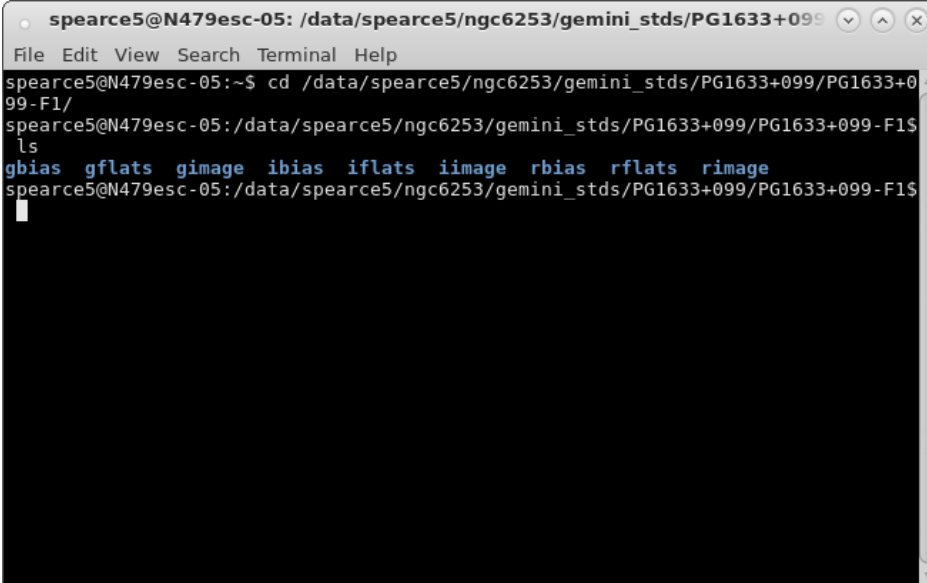
Figure 3.3 Standardized color magnitude diagram of NGC 6253, with the main sequence isochrone fit shown in red. Note that in the center of the plot, the isochrone seems to deviate from the main body of stars. However, the stars in the center of the plot are mostly foreground or background stars, not cluster member, and so were not used in the isochrone fit. Also note that in the lower left corner, the blue line shows the theoretical locations of the cluster white dwarfs if the cluster were 3.5 Gyr, and the red line shows the dimmer population if the cluster were 4.6 Gyr, as our results found.

Appendix A

Data Reduction in THELI

This appendix describes the process I used to reduce Gemini images in THELI, as well as some suggestions for others who may use it in the future.

First, I made directories with subdirectories for the bias frames, flat frames, and images to be reduced, as in Figure A.1. If I had needed to apply dark frames, I would have included subdirectories for them as well.



```
spearce5@N479esc-05: /data/spearce5/ngc6253/gemini_stds/PG1633+099
File Edit View Search Terminal Help
spearce5@N479esc-05:~$ cd /data/spearce5/ngc6253/gemini_stds/PG1633+099/PG1633+099-F1/
spearce5@N479esc-05:/data/spearce5/ngc6253/gemini_stds/PG1633+099/PG1633+099-F1$
ls
gbias  gflats  gimage  ibias  iflats  iimage  rbias  rflats  rimage
```

Figure A.1 Example directory for use in THELI

Within Theli, I simply followed the tabs along the top and performed the tasks in each.

In the first tab, labeled "Initialise", I entered the project name, the directory pathway, and the subdirectories with the data to be used. I also selected the GMOS-S@GEMINI instrument from the list. Between each run in Theli, I clicked the "Reset" button in this tab to prepare for a new set of data.

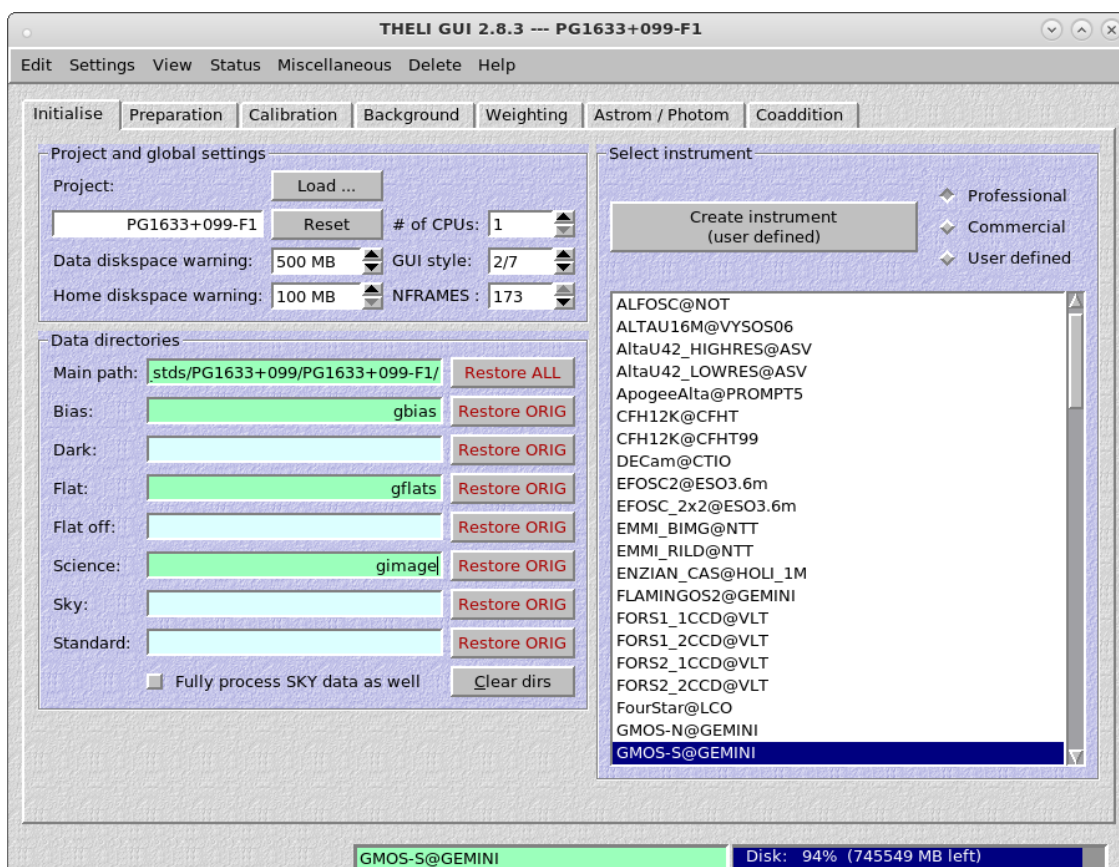


Figure A.2 Initialise tab within THELI, with a project name entered and the directories set.

In the next tabs, I performed each task labeled in red (the other tasks were not required for my needs) by checking the box and pressing "Start".

The second tab, labeled "Preparation", is used to "Split FITS / correct header", which separates the Gemini fits file into three fits images (one for each chip), and applies the header file to each.

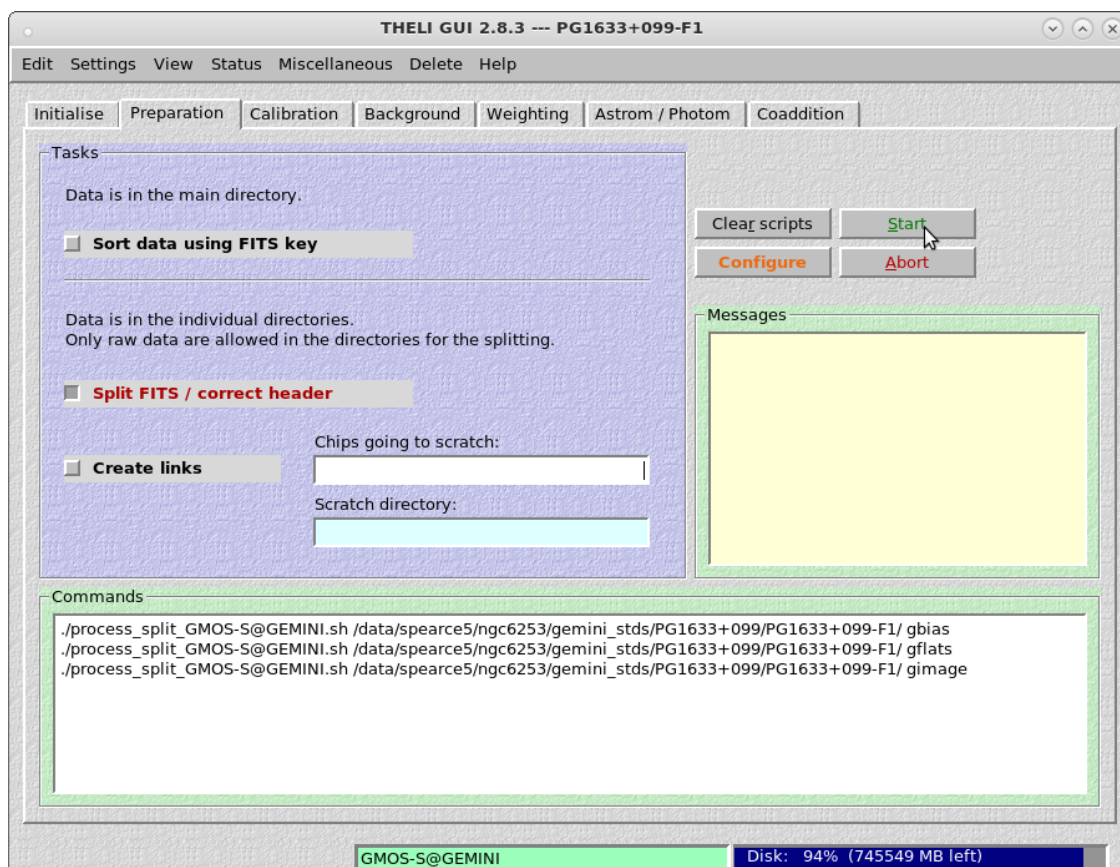


Figure A.3 Preparation tab within THELI, with box "Split FITS / correct header" marked.

The third tab, "Calibration", is used to perform the bias, dark, and flat corrections, and calibrate the data. Since I was not using dark frame subtraction, I did not mark that box.

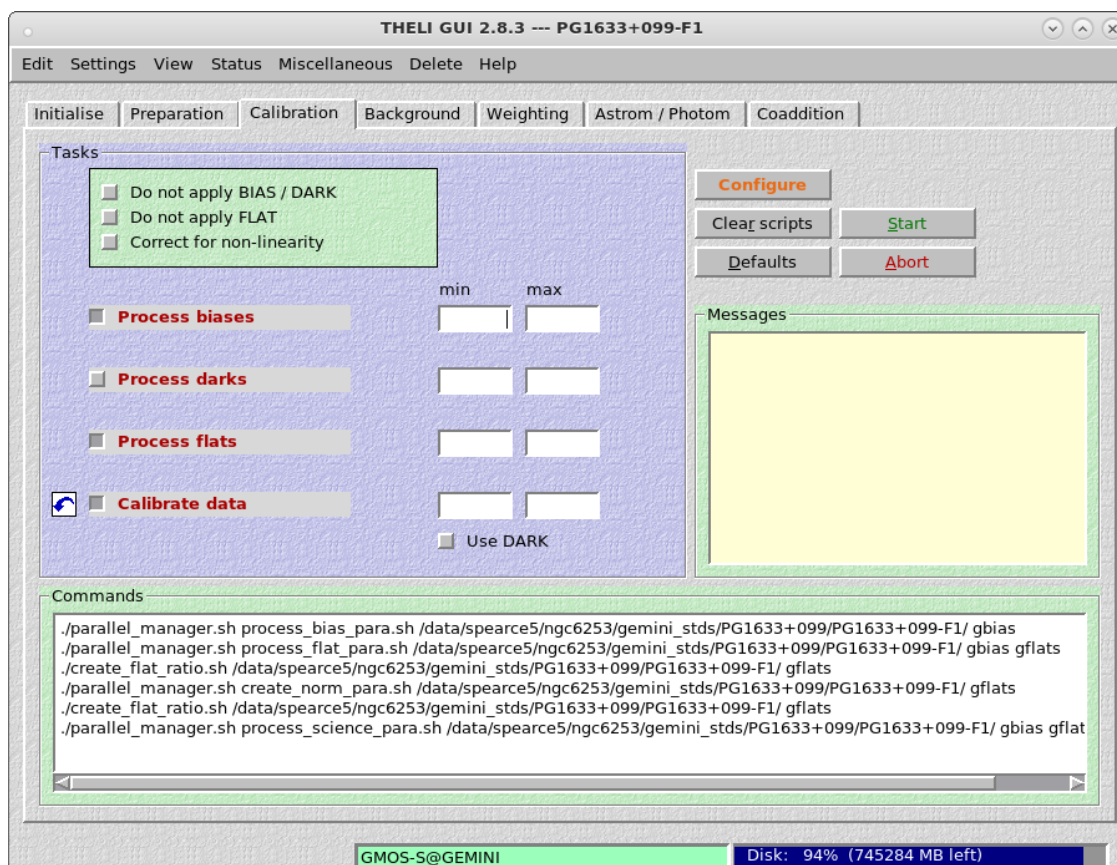


Figure A.4 Calibration tab within THELI, with boxes checked for bias and flat corrections, and data calibration.

The fourth tab, "Background", performs background corrections which were not necessary for my data reductions.

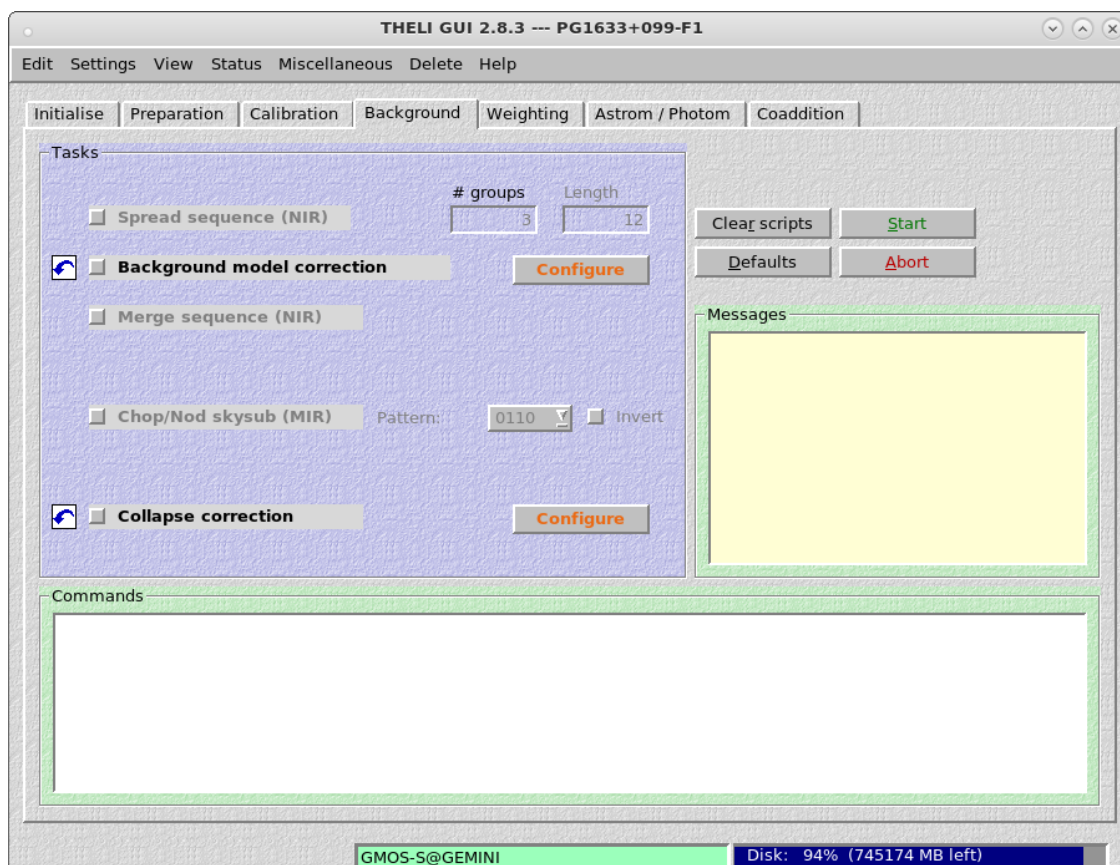


Figure A.5 Background tab within THELI.

The fifth tab, "Weighting", determines the individual weights of the images for the coaddition.

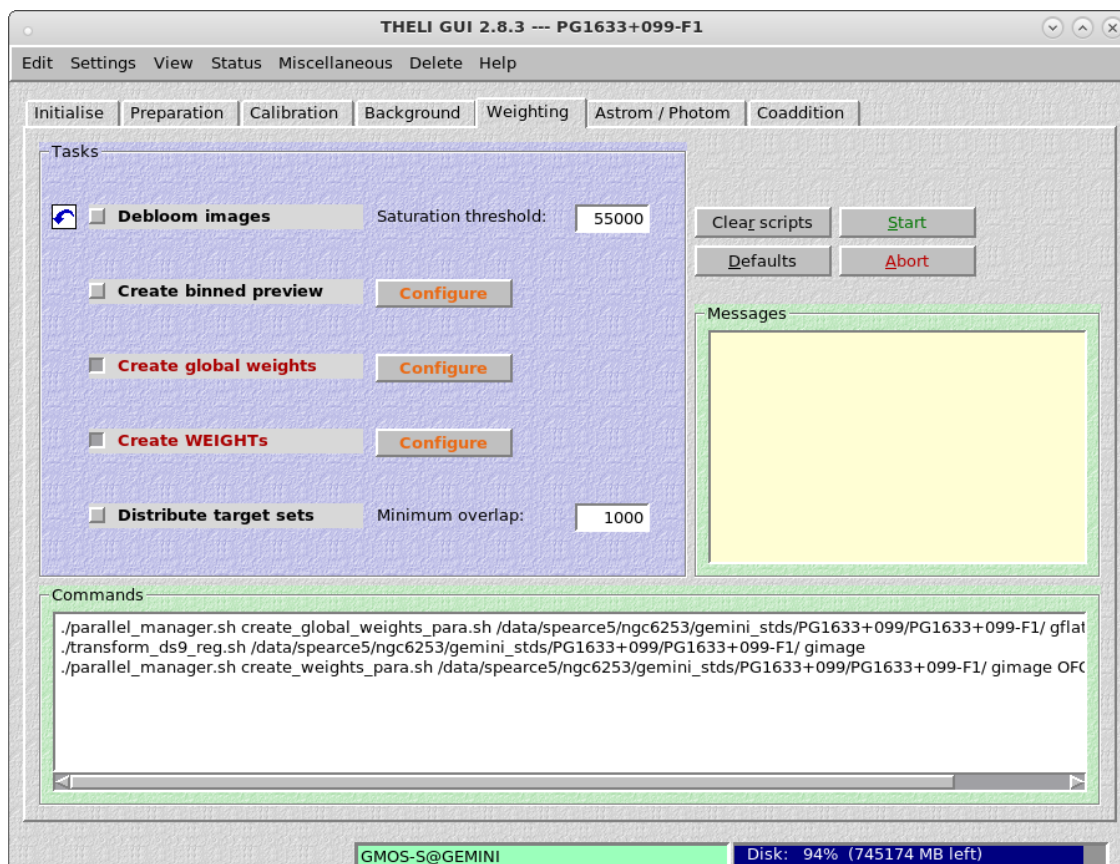


Figure A.6 Weighting tab within THELI, with boxes checked to create the weights for coadditions.

The sixth tab, "Astrom / Photom", obtains the astrometric and photometric solutions. Before checking the boxes, I first get a star catalog by clicking the "Get Catalog" button, adjusting the parameters as needed.

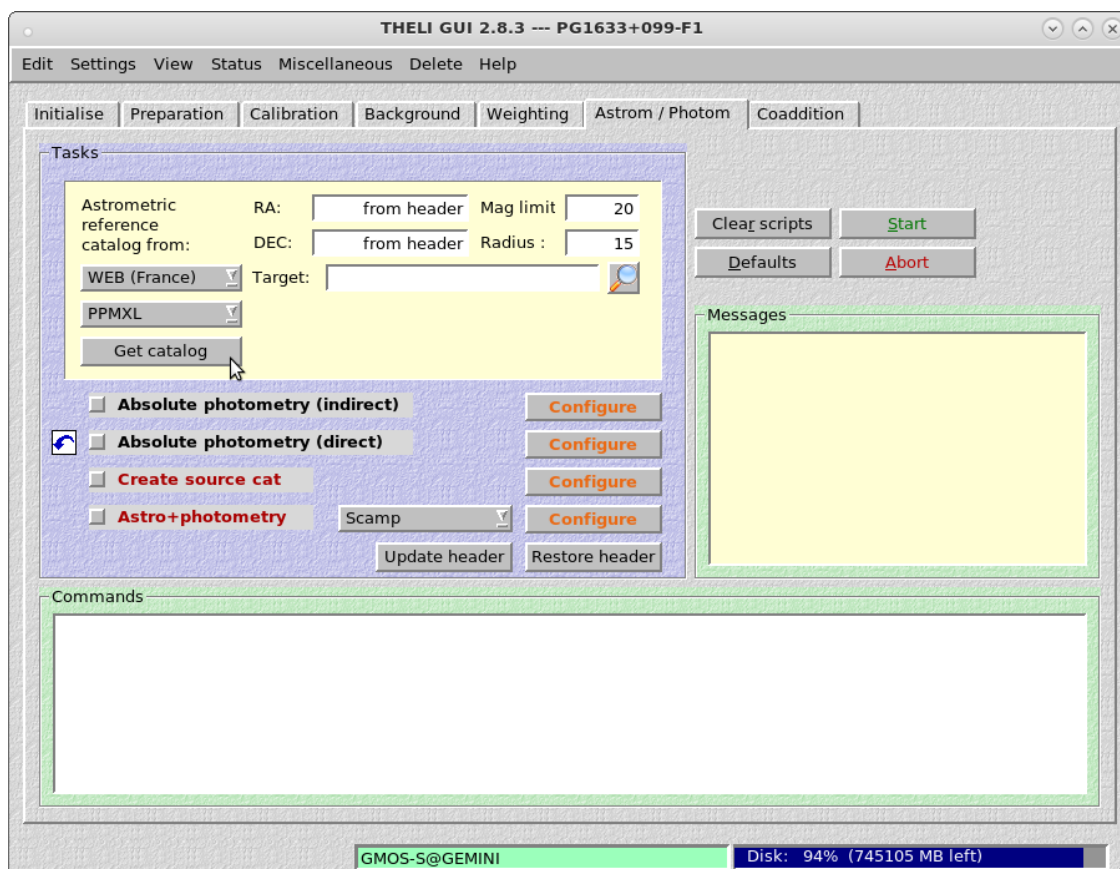


Figure A.7 Astrom / Photom tab within THELI, with the cursor over the "Get Catalog" button.

In this tab, I also needed to configure the Create Source Cat and the Astro+Photometry tasks by clicking the configure buttons to the right of the check boxes for those tasks. The parameters I set are shown in Figures A.8 and A.9.

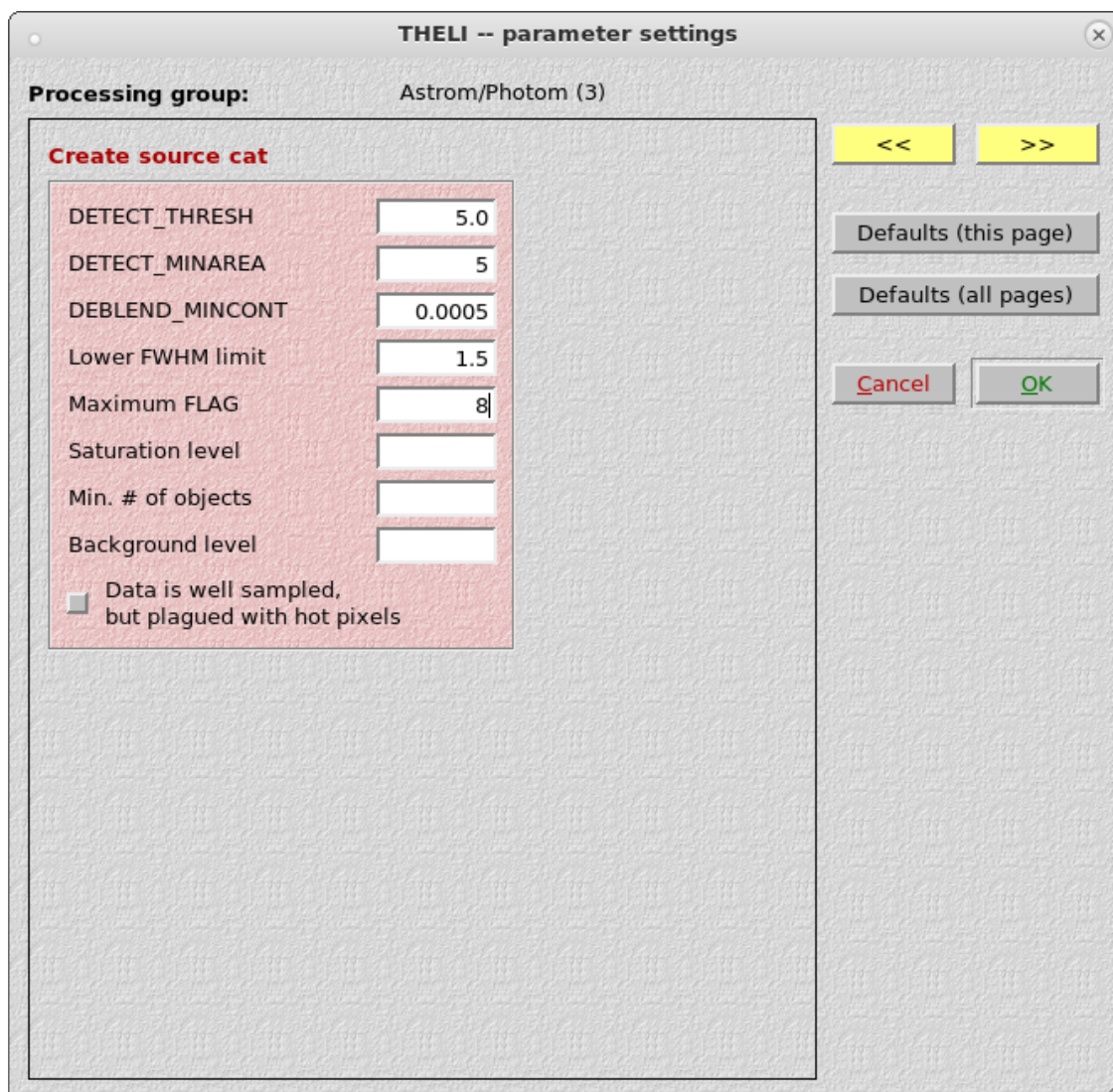


Figure A.8 Parameters used for the Create Source Cat task.

THELI -- parameter settings

Processing group: Astrom/Photom (4)

Astro+photometry

Scamp | Astrometry.net

POSANGLE_MAXERR (deg)	180
POSITION_MAXERR (arcmin)	5.0
PIXSCALE_MAXERR (factor)	1.15
DISTORT_DEGREES	3
FGROUP_RADIUS (deg)	1.0
CROSSID_RADIUS (arcsec)	1.4
ASTREF_WEIGHT	1.0
SN_THRESHOLDS (low high)	5 20
Add. DISTORT_GROUPS DEGREES	
Additional DISTORT_KEYS	
ASTRINSTRU_KEY	NONE
PHOTINSTRU_KEY	NONE
STABILITY_TYPE	INSTRUMENT
MOSAIC_TYPE	README UNCHANGED
FOCAL_PLANE	Use default FP

Match flipped images

<< >>

Defaults (this page)

Defaults (all pages)

Cancel OK

Figure A.9 Parameters used for the Astro+Photometry task.

After setting the parameters, I ran the Create source cat and Astro+Photometry tasks. After performing the Astro+Photometry task on our system, an error message appears, which stems from the program trying to call another program which our computers do not have. This does not affect the the data reductions, so it is fine to move on to the last tab.

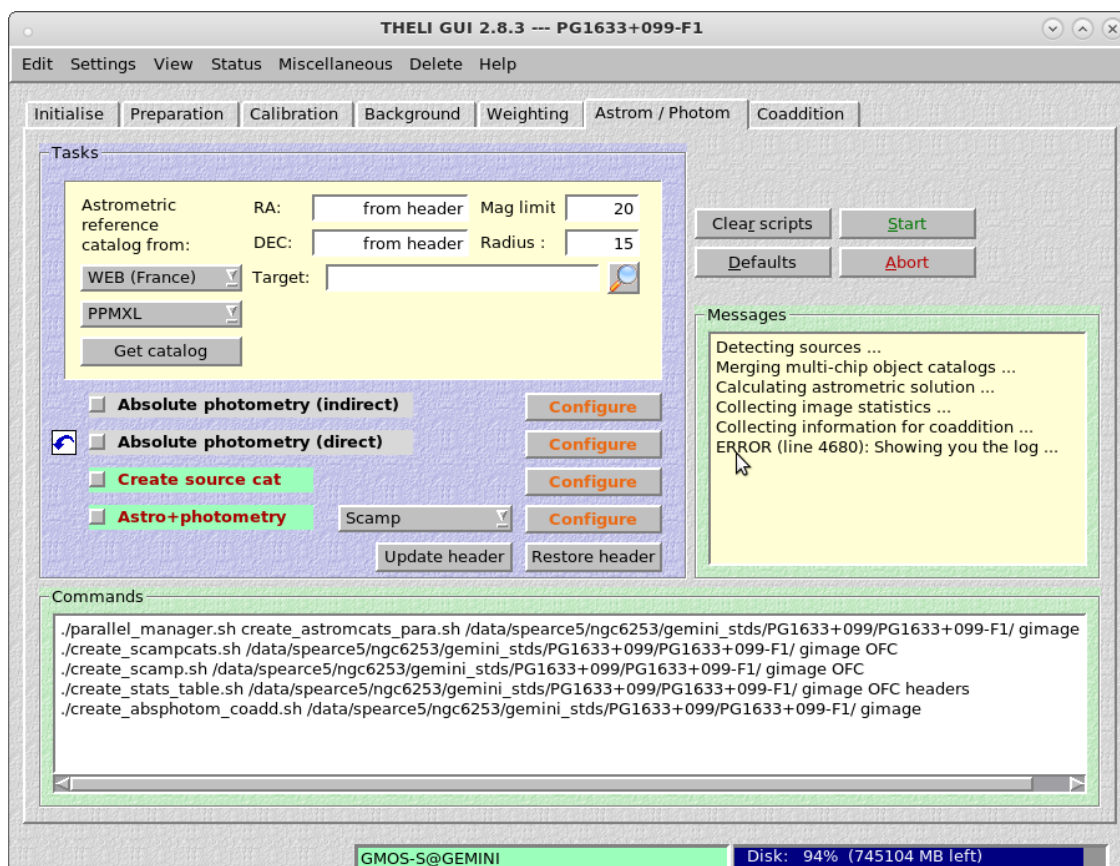


Figure A.10 Astrom / Photom tab within THELI, with error code in the message box.

The final tab, "Coaddition", mosaics the images from the three chips into one. After performing the tasks here, another error message like the one in the previous tab appears, but again, it does not affect the data reduction.

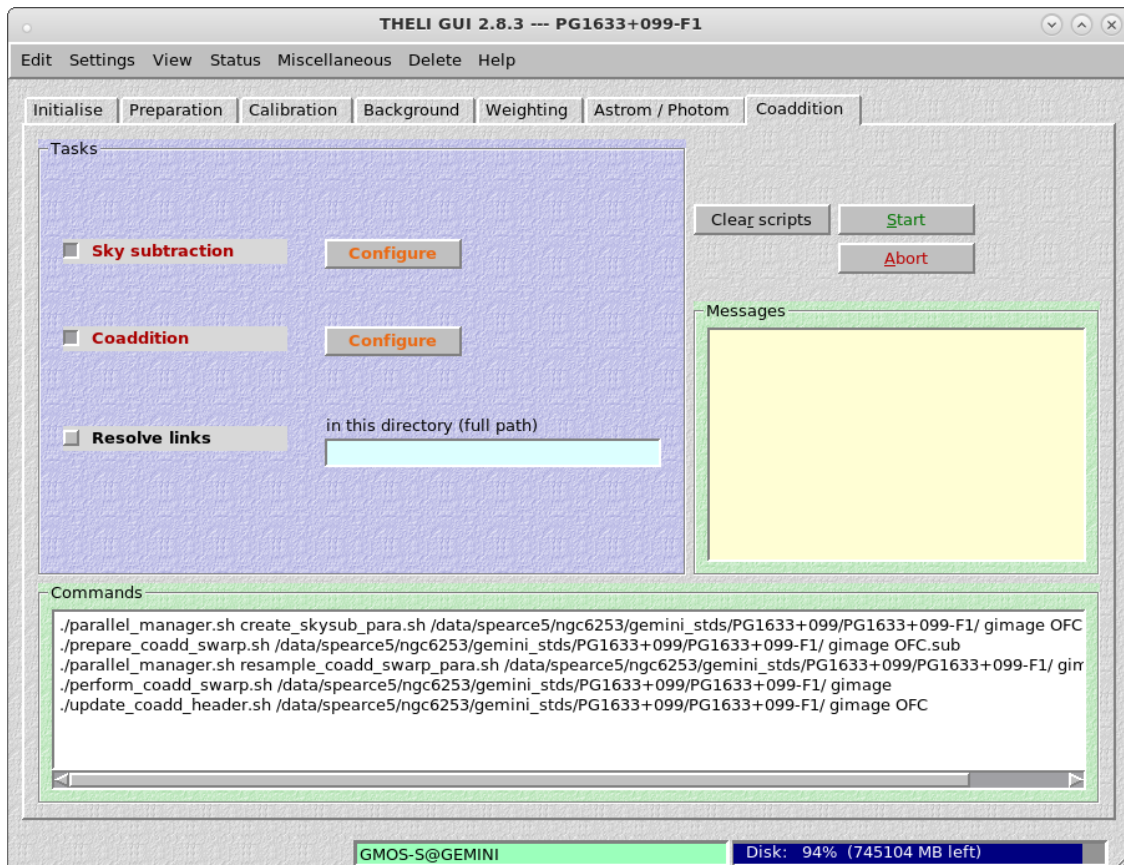
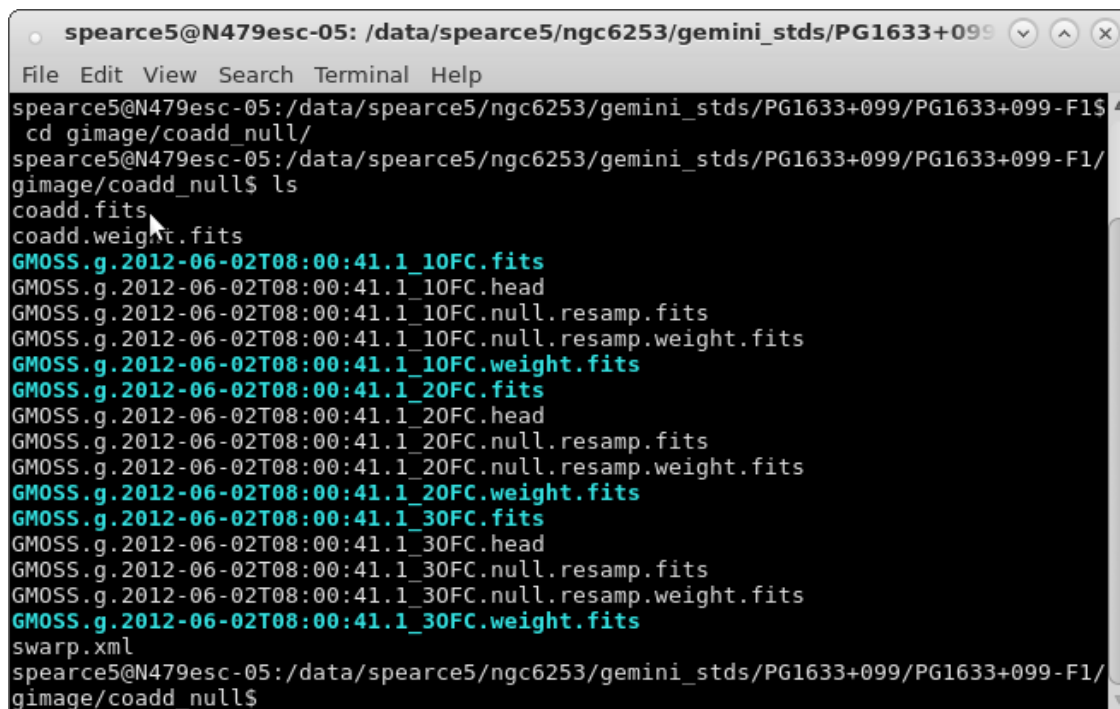


Figure A.11 Coaddition tab within THELI, with boxes checked for sky subtraction and coaddition.

After completing those tasks, the reduced fits file will be found in a new subdirectory, called "coadd_null", in the image subdirectory. The image is labeled "coadd.fits". Also note, all of the original files used will be in new subdirectories labeled "ORIGINALS" within their starting subdirectories.



```
spearce5@N479esc-05: /data/spearce5/ngc6253/gemini_stds/PG1633+099
File Edit View Search Terminal Help
spearce5@N479esc-05:/data/spearce5/ngc6253/gemini_stds/PG1633+099/PG1633+099-F1$
cd gimage/coadd_null/
spearce5@N479esc-05:/data/spearce5/ngc6253/gemini_stds/PG1633+099/PG1633+099-F1/
gimage/coadd_null$ ls
coadd.fits
coadd.weight.fits
GMOSS.g.2012-06-02T08:00:41.1_10FC.fits
GMOSS.g.2012-06-02T08:00:41.1_10FC.head
GMOSS.g.2012-06-02T08:00:41.1_10FC.null.resamp.fits
GMOSS.g.2012-06-02T08:00:41.1_10FC.null.resamp.weight.fits
GMOSS.g.2012-06-02T08:00:41.1_10FC.weight.fits
GMOSS.g.2012-06-02T08:00:41.1_20FC.fits
GMOSS.g.2012-06-02T08:00:41.1_20FC.head
GMOSS.g.2012-06-02T08:00:41.1_20FC.null.resamp.fits
GMOSS.g.2012-06-02T08:00:41.1_20FC.null.resamp.weight.fits
GMOSS.g.2012-06-02T08:00:41.1_20FC.weight.fits
GMOSS.g.2012-06-02T08:00:41.1_30FC.fits
GMOSS.g.2012-06-02T08:00:41.1_30FC.head
GMOSS.g.2012-06-02T08:00:41.1_30FC.null.resamp.fits
GMOSS.g.2012-06-02T08:00:41.1_30FC.null.resamp.weight.fits
GMOSS.g.2012-06-02T08:00:41.1_30FC.weight.fits
swarp.xml
spearce5@N479esc-05:/data/spearce5/ngc6253/gemini_stds/PG1633+099/PG1633+099-F1/
gimage/coadd_null$
```

Figure A.12 The new coadd_null subdirectory, showing the new coadd.fits reduced image file.

For more complete information, the THELI manual (Schirmer 2013) can be found at <https://www.astro.uni-bonn.de/theli/gui/>.

Bibliography

Althaus, L. G., Garcia-Berro, E., Renedo, I., Isern, J., Corsico, A. H., & Rohrmann, R. D. 2010, *ApJ*, 719, 612

Anthony-Twarog, B. J., Deliyannis, C. P., Twarog, B. A., Cummings, J. D., & Maderak, R. M. 2010, *AJ*, 19, 2034

Bedin, L. R., King, I. R., Anderson, J., Piotto, G., Salaris, M., Cassisi, S., & Serenelli, A. 2008, *ApJ*, 678, 1279

Bekki, K. 2011, *MNRAS*, 412, 2241

Carraro, G., Villanova, S., Demarque, P., McSwain, M. V., Piotto, G., & Bedin, L. R. 2006, *ApJ*, 643, 1151

de Marchi, F., Poretti, E., Montalto, M., Desidera, S., & Piotto, G. 2010, *A&A*, 509, 18

Dotter, A., Chaboyer, B., Jevremović, D., Kostov, V., Baron, E., & Ferguson, J. W. 2008, *ApJS*, 178, 89

Durrell, P. R., & Harris, W. E. 1993, *AJ*, 105, 1420

ESO. Accessed 26 August 2017, <https://www.eso.org/public/images/eso0728c/>

Feng, Y., & Krumholz, M. R. 2014, *Nature*, 513, 523

- Garcia-Berro, E., & Oswalt, T. D. 2016, *New A Rev.*, 72, 1
- García-Berro, E., et al. 2010, *Nature*, 465, 194
- Gratton, R., Bragaglia, A., Carretta, E., & Tosi, M. 2006, *ApJ*, 642, 462
- Harris, H. C., et al. 2006, *AJ*, 131, 571
- Kaluzny, J., Rozyczka, M., Pych, W., & Thompson, I. B. 2014, *Acta Astron.*, 64, 77
- Leggett, S. K., Ruiz, M. T., & Bergeron, P. 1998, *ApJ*, 497, 294
- Liebert, J., Bergeron, P., & Holberg, J. B. 2005, *ApJS*, 156, 47
- Milone, A. P., Marino, A. F., D'Antona, F., Bedin, L. R., Costa, G. S. D., Jerjen, H., & Mackey, A. D. 2016, *MNRAS*, 458, 4368
- Montalto, M., Piotto, G., Desidera, S., Platais, I., Carraro, G., Momany, Y., de Marchi, F., & Recio-Blanco, A. 2009, *A&A*, 505, 1129
- Origlia, L., Valenti, E., Rich, R. M., & Ferraro, F. R. 2006, *ApJ*, 646, 499
- Rozyczka, M., Kaluzny, J., Thompson, I. B., Dotter, A., Pych, W., & Narloch, W. 2014, *Acta Astron.*, 64, 233
- Schirmer, M. 2013, *ApJS*, 209, 16
- Smith, J. A., Allam, S. S., Douglas, L. T., Stute, J. L., Rodgers, C. T., & Stoughton, C. 2007, *AJ*, submitted
- von Hippel, T., Jefferys, W. H., Scott, J., Stein, N., Winget, D. E., De Gennaro, S., Dam, A., & Jeffery, E. 2006, *ApJ*, 645, 1436

von Hippel, T., van Dyk, D. A., Stenning, D. C., Robinson, E., Jeffery, E., Stein, N., Jefferys, W. H., & O'Malley, E. 2014, in EAS Publications Series, Vol. 65, EAS Publications Series, 267–287